Condensate fraction and momentum distribution in the ground state of liquid ^{4}He

E. Manousakis, V. R. Pandharipande, and Q. N. Usmani*
Department of Physics and Materials Research Laboratory, University of Illinois at Urbana-Champaign, 1110 West Green Street, Urbana, Illinois 61801
(Received 5 October 1984)

Calculations of the condensate fraction and momentum distribution of liquid ^{4}He are carried out using variational ground-state wave functions containing two-body (Jastrow) and three-body correlations. These wave functions give a satisfactory description of the equation of state of the liquid at $T=0$. The calculations are performed within the scheme of hypernetted-chain equations, using the scaling approximation for evaluating the contributions of the elementary diagrams. Results are reported at densities $\rho=0.365\sigma^{-3}$, $0.401\sigma^{-3}$, and $0.438\sigma^{-3}$, and compared with momentum distributions obtained from experimental data and Green's-function Monte Carlo calculations.

I. INTRODUCTION

The theoretical and experimental studies of condensate fraction and momentum distribution of atoms in liquid ^{4}He are a longstanding problem of fundamental interest. These studies started four decades ago after London[1] proposed a connection between the λ transition and the Bose-Einstein condensation. In recent years, a variety of experimental techniques[2–4] have been employed to measure the momentum distribution in helium liquids. At the equilibrium density, analysis of the experimental data[2,3] gives condensate fraction $n_0 \sim 9$–$13\,\%$ at $T=0$. The value of n_0 obtained from the Green's-function Monte Carlo (GFMC) calculations[5] using the HFDHE2 interatomic potential of Aziz *et al.*[6] is found to be 9%, which is at the lower limit of the experimental value. The value of the average kinetic energy per atom has also been inferred from the experimental data.[3] The experimental value of 14.0 ± 0.5 K is in reasonable agreement with that obtained in GFMC (14.5 K) and variational[7] (14.8 K) calculations.

The momentum distribution $n(k)$ is generally obtained by calculating the one-body density matrix $\rho(r_{11'})$, and taking its Fourier transform.[8] It is known[9] that to obtain an accurate evaluation of the $\rho(r_{11'})$, with chain summation methods, it is necessary to sum the various series of elementary diagrams. Fabrocini and Rosati[10] used the method of interpolating between the hypernetted-chain (HNC) and Percus-Yevick (PY) equations to calculate $n(k)$. In this paper we generalize the scaling method (HNC/S) developed earlier[11,7] for the calculation of two- and three-particle distribution functions, to sum the series of elementary diagrams in the calculation of $\rho(r_{11'})$.

During the course of this work Puoskari and Kallio[12] (PK) have also calculated the $\rho(r_{11'})$ with a very similar HNC/S method. They have used Jastrow variational wave functions

$$\Psi_J = \sum_{i<j} f(r_{ij}) , \tag{1.1}$$

obtained with the Lennard-Jones potential, whereas we use the more realistic wave functions

$$\Psi_v = \prod_{i<j} f(r_{ij}) \prod_{i<j<k} f_3(r_{ij},r_{jk},r_{ki}) \tag{1.2}$$

containing three-particle correlations. Our wave functions are obtained from the Aziz potential[6] which gives a better equation of state than the Lennard-Jones potential.[5]

The HNC/S equations of the $\rho(r_{11'})$ of a Jastrow wave function are given in Sec. II. The small differences between PK and our formalism are discussed at the end of this section. The results of HNC/S calculations for the McMillan-Jastrow wave function are reported; these are in excellent agreement with the exact Monte Carlo results.[13]

The HNC/S equations for wave functions containing two- and three-body correlations are given in Sec. III. The $n(k)$ calculated from the best available variational wave functions (those of Ref. 7) is reported in Sec. IV. Our values of n_0 are similar to those obtained with the GFMC method, and a little below those obtained from the analysis of neutron scattering data. The density dependence of n_0 and $n(k)$ is discussed.

II. HNC/S METHOD FOR JASTROW WAVE FUNCTION

The one-particle density matrix is defined as

$$\rho(\mathbf{r}_{11'}) = N \frac{\int \Psi^*(\mathbf{r}_{1'},\mathbf{r}_2,\ldots,\mathbf{r}_N)\Psi(\mathbf{r}_1,\mathbf{r}_2,\ldots,\mathbf{r}_N)d^3r_2\cdots d^3r_N}{\int |\Psi(\mathbf{r}_1,\ldots,\mathbf{r}_N)|^2 d^3r_1\cdots d^3r_N} , \tag{2.1}$$

where N is the total number of particles in the liquid and $\mathbf{r}_{11'}=\mathbf{r}_1-\mathbf{r}_{1'}$. In homogeneous liquids ($N\to\infty$, at constant density) the $\rho(r_{11'})$ is a function of $|\mathbf{r}_{11'}|$ only. Its Fourier transform gives the occupation probability for single-particle states with momentum k:

$$n(k)=\int \rho(r)e^{i\mathbf{k}\cdot\mathbf{r}}d^3r \ . \tag{2.2}$$

In Bose systems $n(k)$ is written as

$$n(k)=Nn_0\delta_{k,0}+\int [\rho(r)-\rho(r\to\infty)]e^{i\mathbf{k}\cdot\mathbf{r}}d^3r \ , \tag{2.3}$$

where n_0 is the condensate fraction, and the second term represents the momentum distribution for $k>0$.

By expanding the many-body integrals in Eq. (2.1), in powers of the functions

$$h(r_{ij})=f^2(r_{ij})-1 \ , \qquad \zeta(r_{ij})=f(r_{ij})-1 \ , \tag{2.4}$$

the following irreducible structure for the one-particle density matrix has been obtained:[8]

$$\rho(r)=\rho n_0\exp[N_{ww}(r)+E_{ww}(r)] \ . \tag{2.5}$$

Here ρ is the number density of the liquid and $N_{ww}(r)$ is the sum of nodal diagrams given by the convolution

$$N_{ww}(r_{11'})=\rho\int d^3r_2[g_{wd}(r_{12})-1]\times[g_{wd}(r_{1'2})-N_{wd}(r_{1'2})-1] \ . \tag{2.6}$$

The functions $g_{wd}(r)$ and $N_{wd}(r)$ are obtained by solving the HNC equations

$$g_{wd}(r_{12})=f(r_{12})\exp[N_{wd}(r_{12})+E_{wd}(r_{12})] \ , \tag{2.7}$$

$$N_{wd}(r_{12})=\rho\int d^3r_3[g_{wd}(r_{13})-1]\times[g_{dd}(r_{32})-N_{dd}(r_{32})-1] \ . \tag{2.8}$$

The functions $g_{dd}(r)$ and $N_{dd}(r)$ are the familiar pair-distribution and nodal functions denoted by $g(r)$ and $N(r)$ in Ref. 7.

The condensate fraction n_0 is given by[8]

$$n_0=\exp(2R_w-R_d) \ , \tag{2.9}$$

where

$$R_w=\rho\int d^3r[g_{wd}(r)-1-N_{wd}(r)-E_{wd}(r)]-\tfrac{1}{2}\rho\int d^3r[g_{wd}(r)-1][N_{wd}(r)+2E_{wd}(r)]+E_w \ . \tag{2.10}$$

The R_d is obtained by replacing all the w subscripts in the above equation by d.

The $E_{ww}(r)$, $E_{wd}(r)$, $E_{dd}(r)$, E_w, and E_d represent the contribution of elementary diagrams. There is no analytic method available to evaluate these functions. The lowest order (HNC/0) approximation is characterized by setting all these functions equal to zero. In the HNC/4 approximation the E's are calculated from the four-point elementary diagrams shown in Fig. 1. The dashed straight and wavy lines in these diagrams represent, respectively, $g_{dd}-1$ and $g_{wd}-1$. The solid and open circles represent internal and external points. The contributions of these diagrams are given by

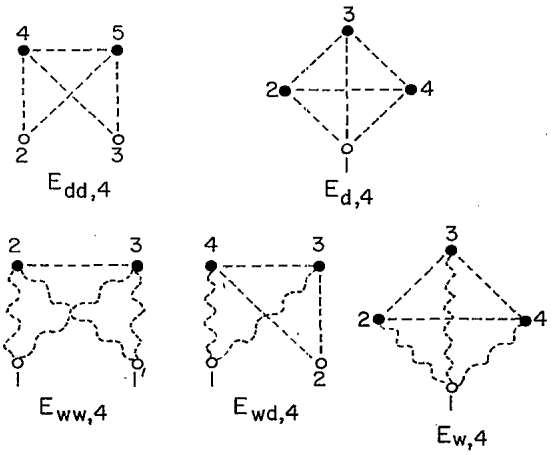

FIG. 1. Four-point elementary diagrams.

$$E_{ww,4}(r_{11'})=\tfrac{1}{2}\rho^2\int (g_{wd}-1)_{12}(g_{wd}-1)_{13}\times(g_{wd}-1)_{1'2}(g_{wd}-1)_{1'3}\times(g_{dd}-1)_{23}d^3r_2d^3r_3 \ , \tag{2.11a}$$

$$E_{wd,4}(r_{12})=\tfrac{1}{2}\rho^2\int (g_{wd}-1)_{13}(g_{wd}-1)_{14}\times(g_{dd}-1)_{23}(g_{dd}-1)_{24}\times(g_{dd}-1)_{34}d^3r_3d^3r_4 \ , \tag{2.11b}$$

$$E_{dd,4}(r_{23})=\tfrac{1}{2}\rho^2\int (g_{dd}-1)_{24}(g_{dd}-1)_{25}\times(g_{dd}-1)_{34}(g_{dd}-1)_{35}\times(g_{dd}-1)_{45}d^3r_4d^3r_5 \ , \tag{2.11c}$$

$$E_{w,4}=\frac{\rho}{3}\int (g_{wd}-1)_{12}E_{wd,4}(r_{12})d^3r_{12} \ , \tag{2.11d}$$

$$E_{d,4}=\frac{\rho}{3}\int (g_{dd}-1)_{12}E_{dd,4}(r_{12})d^3{}_{12} \ . \tag{2.11e}$$

In the HNC/S method[11] we assumed that

$$E_{dd}(r)\approx(1+s_{dd})E_{dd,4}(r) \ . \tag{2.12}$$

This approximation is based on the observation that the contributions of higher-order elementary diagrams, containing five or more points, have approximately the same spatial behavior as that of $E_{dd,4}(r)$. The scaling constant s_{dd} is determined by fulfilling identities that are valid when the elementary diagrams are summed to all orders.

We note in Fig. 2 that the structure of g_{wd} is similar to that of g_{dd}, and the topological structure of five- and higher-body E_{ww} and E_{wd} diagrams is identical to that of E_{dd} diagrams. In fact E_{wd} (E_{ww}) diagrams are obtained from the E_{dd} diagrams by replacing all the $g_{dd}-1$ bonds from one (both) external point by $g_{wd}-1$ bonds. We thus expect the higher-body wd and ww elementary diagrams to have the same spatial behavior as that of $E_{wd,4}$ and $E_{ww,4}$, respectively, and approximate the total E_{wd} and E_{ww} as follows:

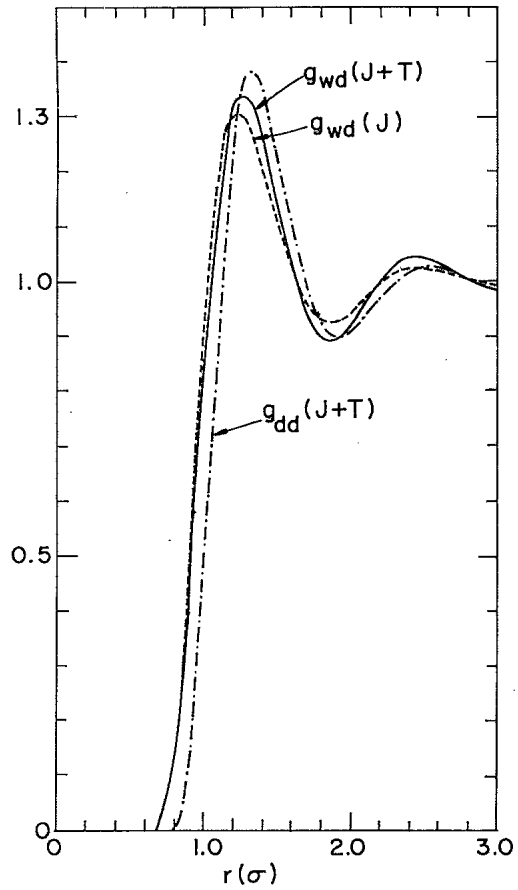

FIG. 2. $g_{xy}(r)$ for Jastrow and J + T wave functions of Ref. 7 at $\rho=0.365\ \sigma^{-3}$.

$$E_{wd}(r)\approx(1+s_{wd})E_{wd,4}(r)\ ,$$
$$E_{ww}(r)\approx(1+s_{ww})E_{ww,4}(r)\ . \tag{2.13}$$

The one-point elementary diagrams give a factor $\exp(2E_w-E_d)$ in the expression for n_0 [Eq. (2.9)]. This factor is neglected in all the earlier work. In HNC/4 approximation $(2E_{w,4}-E_{d,4})$ is of order 0.01, and thus this factor can be safely neglected. We can, of course, scale the $E_{d,4}$ and $E_{w,4}$ to approximate the total E_d and E_w. The E_d and E_w diagrams are obtained by dressing the E_{dd} and E_{wd} diagrams with $g_{dd}-1$ and $g_{wd}-1$, respectively, and integrating over one particle. However, the symmetry factors of the one- and two-point diagrams are generally different, and hence the scaling factors of the one- and two-point diagrams are different, but related. This is very similar to the scaling of three-point Abe diagrams A, and that of the E_{dd}. In Ref. 11 we argued that the ratio of s_{dd} to s_a, the scaling constant for Abe diagrams, is ~ 2. Similar arguments suggest that the ratios s_d/s_{dd} and s_w/s_{wd} should be $\sim\frac{3}{2}$. We, hence, approximate the one-point elementary diagrams as follows:

$$E_d\approx(1+\tfrac{3}{2}s_{dd})E_{d,4}\ ,$$
$$E_w\approx(1+\tfrac{3}{2}s_{wd})E_{w,4}\ . \tag{2.14}$$

We find that $2E_w-E_d$ is ~ 0.03, and thus not very important.

The kinetic energy and normalization identities are used to determine the scaling constants s_{dd}, s_{wd}, and s_{ww}. These are

$$T_{\rm MD}=T_{\rm JF}=T_{\rm PB}\ , \tag{2.15}$$

$$T_{\rm MD}=\int\frac{d^3k}{(2\pi)^3\rho}\frac{\hbar^2}{2m}k^2n(k)\ , \tag{2.16}$$

$$T_{\rm JF}=-\frac{\hbar^2}{4m}\rho\int g_{dd}(r)\left[\frac{\nabla^2 f}{f}-\frac{(\nabla f)^2}{f^2}\right]d^3r\ , \tag{2.17}$$

$$T_{\rm PB}=-\frac{\hbar^2}{2m}\rho\int g_{dd}(r)\frac{\nabla^2 f}{f}d^3r -\frac{\hbar^2}{2m}\rho^2\int g_3(r_{12},r_{13},r_{23})\frac{\nabla_1 f(r_{12})\cdot\nabla_1 f(r_{13})}{f(r_{12})f(r_{13})} \times d^3r_{12}d^3r_{13}\ , \tag{2.18}$$

for the kinetic energy per atom. The subscripts MD, JF, and PB denote momentum-distribution, Jackson-Feenberg, and Pandharipande-Bethe expressions. The normalization condition

$$\int\frac{d^3k}{(2\pi)^3\rho}n(k)=1\ , \tag{2.19}$$

is equivalent to

$$\rho(r_{11'}=0)=\rho\ . \tag{2.20}$$

In Refs. 11 and 7 the identity $T_{\rm PB}=T_{\rm JF}$ is used to determine the s_{dd}. Here we use $T_{\rm MD}=T_{\rm JF}$, and normalization Eq. (2.20) to determine the s_{wd} and s_{ww}. The numerical work is simplified by assuming that $n(k)$ is exponential for $k>3.5$ Å^{-1},

$$n(k>3.5\ \text{Å}^{-1})=\exp[\alpha(k-3.5)]n(k=3.5)\ . \tag{2.21}$$

The constant α is determined by fitting the $\ln[n(k)]$ in $k=3$ to 3.5 Å^{-1} interval to a straight line. This approximation has been verified to be good up to ~ 4 Å^{-1} (see Fig. 7 in Sec. IV). The $k>3.5$ Å^{-1} region gives less than 5% (1%) contribution to $T_{\rm MD}$ [normalization integral (2.19)].

The results obtained with the McMillan correlation:

$$f(r)=\exp[-\tfrac{1}{2}(b/r)^5] \tag{2.22}$$

with $b=1.17\sigma$, at the equilibrium density, are shown in Table I and Fig. 3. The importance of the elementary diagram contributions is obvious. The close agreement between the HNC/S and Monte Carlo results of Refs. 13 and 14 suggests that the scaling approximations for the

TABLE I. Results with McMillan-Jastrow wave function at $\rho=0.365\sigma^{-3}$.

	HNC/0	HNC/4	HNC/S	MC
n_0	0.112	0.113	0.106	0.105±0.005
$\rho(r=0)/\rho$	1.81	1.52	1.00	1.00
$T_{\rm JF}$ (K)	14.71	14.55	14.10	13.95
$T_{\rm MD}$ (K)	33.20	28.80	14.10	

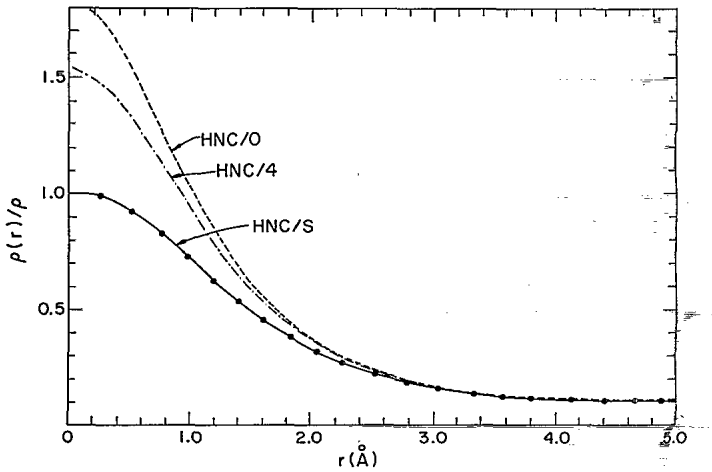

FIG. 3. $\rho(r_{11'})$ for McMillan-Jastrow wave function at $\rho=0.365\sigma^{-3}$ in HNC, HNC/4, and HNC/S approximations. The dots give results of Monte Carlo calculations.

elementary diagrams are quite accurate.

The values of the three scaling factors for the McMillan-Jastrow wave function at equilibrium density are found to be

$$s_{dd}=2.72,\quad s_{wd}=1.71,\quad s_{ww}=1.86\ , \tag{2.23}$$

Puoskari and Kallio[12] use both the two-component mixture and Fantoni's formalism used here to calculate the $\rho(r_{11'})$. At any level of approximation the mixture formalism and Fantoni's $\rho(r_{11'})$ are proportional to each other. The only difference is that in mixture formalism the n_0 is calculated by using the normalization condition (2.20) in Eq. (2.5), whereas Fantoni calculates it independently by Eq. (2.9). PK also use scaling constants s_{dd}, s_{dw}, and s_{ww} (their $\kappa_{\alpha\beta}$ equal $1+s_{\alpha\beta}$ in our notation), and determine them from $T_{\rm JF}=T_{\rm PB}$, $T_{\rm MD}=T_{\rm JF}$, and $T_{\rm MD}$(mixture) $=T_{\rm MD}$ where $T_{\rm MD}$(mixture) is the kinetic energy obtained with $n(k)$ from mixture formalism. This procedure is identical to ours because $n(k)$(mixture) is proportional to $n(k)$, and so $T_{\rm MD}$(mixture)$=T_{\rm MD}$ is identical to the normalization condition. Thus we do not find that the mixture formalism offers any simplification. PK neglect the contribution of one-body elementary diagrams E_d and E_w; we include them, but find that they are small.

III. THREE-BODY CORRELATIONS

A significant improvement in the variational energy of liquid helium is obtained by including three-body correlations in the wave function.[7,15] The wave function (the J + T denotes Jastrow plus triplet) is taken as

$$\Psi_{\rm J+T}=\prod_{i<j}f(r_{ij})\prod_{i<j<k}f_3(\mathbf{r}_{ij},\mathbf{r}_{ik})\ , \tag{3.1}$$

$$f_3(\mathbf{r}_{ij},\mathbf{r}_{ik})=\exp\left[-\tfrac{1}{2}\sum_{\rm cyc}\sum_{l=0,2}\xi_l(r_{ij})\xi_l(r_{ik})P_l(\mathbf{r}_{ij}\cdot\mathbf{r}_{ik})\right]\ . \tag{3.2}$$

The $l=1$ term of f_3 gives the dominant contribution, the $l=0$ term gives a small contribution, and the $l=2$ term has negligible effect.[7]

HNC equations for the distribution functions of the J + T wave function have been discussed in Ref. 7. The HNC equations for the density matrix are obtained in an analogous way by replacing the E_{xy},$xy=dd$, wd, and ww as follows:

$$E_{xy}=C_{xy}+E^g_{xy}+E^t_{xy}\ . \tag{3.3}$$

Here C_{xy} are three-body elements given by

$$C_{dd}(r_{ij})=\rho\int[f_3^2(\mathbf{r}_{ia},\mathbf{r}_{ja})-1]\times g_{dd}(r_{ia})g_{dd}(r_{ja})d^3r_a\ , \tag{3.4}$$

$$C_{wd}(r_{1j})=\rho\int[f_3(\mathbf{r}_{1a},\mathbf{r}_{ja})-1]\times g_{wd}(r_{1a})g_{dd}(r_{ja})d^3r_a\ , \tag{3.5}$$

$$C_{ww}(r_{11'})=0\ . \tag{3.6}$$

E^g_{xy} is the sum of elementary diagrams having only $g_{xy}-1$ bonds, and E^t_{xy} is the sum of elementary diagrams having one or more three-body correlations. The $E^t_{dd,4}$ diagrams are given in Fig. 1 of Ref. 7, and $E^t_{wd,4}$, $E^t_{ww,4}$, and $E^t_{w,4}$ diagrams are given in Figs. 4, 5, and 6, respectively. In these diagrams a wiggly line triangle $1jk$ with 1 as an external point represents

$$[f_3(\mathbf{r}_{1j},\mathbf{r}_{1k})-1]g_{wd}(r_{1j})g_{wd}(r_{1k})g_{dd}(r_{jk})\ ,$$

whereas a plain triangle ijk represents

$$[f_3^2(\mathbf{r}_{ij},\mathbf{r}_{ik})-1]g_{dd}(r_{ij})g_{dd}(r_{ik})g_{dd}(r_{jk})\ .$$

As in Ref. 7, a cross on a side ij of the triangle indicates

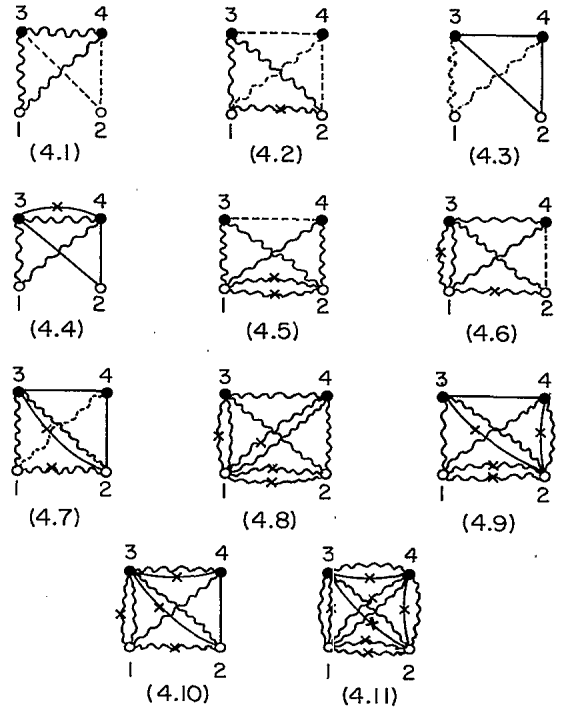

FIG. 4. Four-point E^t_{wd} diagrams.

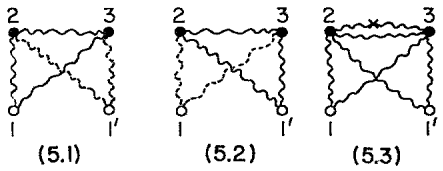

FIG. 5. Four-point E^t_{ww} diagrams.

that the factor g_{wd} or g_{dd} is to be omitted.

The equation (2.10) for $R_x, x=w,d$ becomes

$$R_x=\rho\int d^3r(g_{xd}-1-N_{xd}-C_{xd}-E^g_{xd}-E^t_{xd})$$
$$-\tfrac{1}{2}\rho\int d^3r(g_{xd}-1)(N_{xd}+2E^g_{xd}+2E^{t1}_{xd})$$
$$-\rho\int d^3r g_{xd}(E^{t2}_{xd}+\tfrac{1}{2}C_{xd})+E^g_x+E^t_x\ , \qquad (3.7)$$

where $E^{t2}_{xy}(r)$ $[E^{t1}_{xy}(r)]$ are sums of $E_{xy}(r)$ diagrams that contain [do not contain] a three-body correlation connecting the two external points. For example, diagrams (4.1), (4.3), and (4.4) of Fig. 4 contribute to $E^{t1}_{wd,4}$ while the rest contribute to $E^{t2}_{wd,4}$.

The bonds $g_{dd}(r)-1$ and $g_{wd}(r)-1$ do not change much when three-body correlations are added to the wave function. Thus following Ref. 7 we assume that the scaling factors s_{xy} for the E^g_{xy} do not change by switching on the three-body correlations. The f_3 is set to one and the s_{xy} are calculated as discussed in the preceding section.

The contribution of E^t_{xy} diagrams is generally smaller than that of the E^g_{xy} diagrams. The $E^t_{dd}(r)$ changes sign[7] at $r\sim 0.5\sigma$, and it is unlikely that a scaling approximation for the total E^t_{dd} is valid. Hence in Ref. 7, and in the present work all five or more point E^t_{xy} diagrams are neglected. We also neglect $E^t_{ww,4}$ for reasons discussed later. Thus in practice the f_3 is switched on after completing the Jastrow calculation, and the HNC equations for J + T are solved with E^g_{xy} and E^g_x given by the scaling approximations and

$$E^t_{dd}=E^t_{dd,4},\quad E^t_{wd}=E^t_{wd,4}\ ,$$
$$E^t_w=E^t_{w,4},\quad E^t_d=E^t_{d,4};\quad E^t_{ww}=0\ . \qquad (3.8)$$

At equilibrium density the calculation described above, carried out with the wave function of Ref. 7, gives $T_{\rm MD}=14.8$ K, in close agreement with $T_{\rm JF}=14.72$ K, and normalization $\rho(r_{11'}=0)=0.95\rho$. It thus satisfies the known identities to a reasonable accuracy. However, if we take

$$E^t_{ww}=E^t_{ww,4}\ , \qquad (3.9)$$

the $T_{\rm MD}=18.8$ K and $\rho(r_{11'}=0)=1.065\rho$. The kinetic energy identity is particularly violated, and so it appears that it is better to neglect E^t_{ww} than to approximate it with $E_{ww,4}$. Crude numerical studies of $E^t_{ww,5}$ $(r=0)$ show that at least at $r=0$, $E^t_{ww,5}$ is of the order of magnitude of $E_{ww,4}$ but opposite in sign.

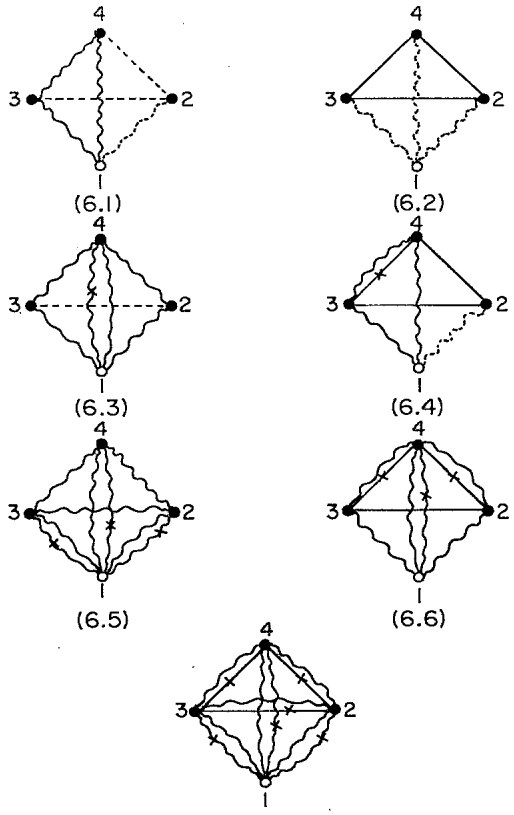

FIG. 6. Four-point E^t_w diagrams.

IV. RESULTS

In this section we present the results obtained with realistic J + T wave functions of Ref. 7 at three densities. In addition to the triplet correlations these wave functions contain an optimized pair correlation having the asymptotic behavior

$$f(r\to\infty)=1-\frac{mc}{2\pi^2\hbar\rho}\frac{1}{r^2}\ , \qquad (4.1)$$

a consequence of the long-wavelength phonons.[16] Here c is the velocity of zero sound. It may be easily verified that this asymptotic behavior of f implies the following asymptotic conditions for the nodal functions:

$$N_{dd}(r\to\infty)=\frac{mc}{\pi^2\hbar\rho}\frac{1}{r^2}\ , \qquad (4.2)$$

$$N_{wd}(r\to\infty)=N_{dd}/2\ , \qquad (4.3)$$

$$N_{ww}(r\to\infty)=N_{dd}/4\ , \qquad (4.4)$$

and the $n(k)$,

$$n(k\to 0)=n_0\frac{mc}{2\hbar}\frac{1}{k}\ . \qquad (4.5)$$

The results of our calculations are given in Tables II and III, and Figs. 7–9. The results of the full calculation are labeled J + T, while those labeled J are obtained on switching off the triplet correlation. The GFMC results are taken from a calculation by Whitlock and Panoff.[17] In all these results $n(k)$ is normalized such that

$$\int n(k)d^3k=1\ . \qquad (4.6)$$

TABLE II. $kn(k)$ with the J + T wave function at various densities.

k (Å^{-1}) \ $\rho(\sigma^{-3})$	0.365	0.401	0.438
0.05	0.0167	0.0136	0.0106
0.25	0.0318	0.0264	0.0208
0.45	0.0416	0.0349	0.0279
0.65	0.0458	0.0391	0.0318
0.85	0.0455	0.0398	0.0331
1.05	0.0417	0.0377	0.0324
1.25	0.0350	0.0332	0.0298
1.45	0.0264	0.0266	0.0253
1.65	0.0175	0.0190	0.0196
1.85	0.0112	0.0129	0.0144
2.05	0.0091	0.0105	0.0117
2.25	0.0084	0.0097	0.0109
2.45	0.0066	0.0080	0.0094
2.65	0.0045	0.0058	0.0072
2.85	0.0029	0.0041	0.0054
3.05	0.0019	0.0027	0.0039
3.25	0.0012	0.0018	0.0027
3.35	0.0007	0.0011	0.0019

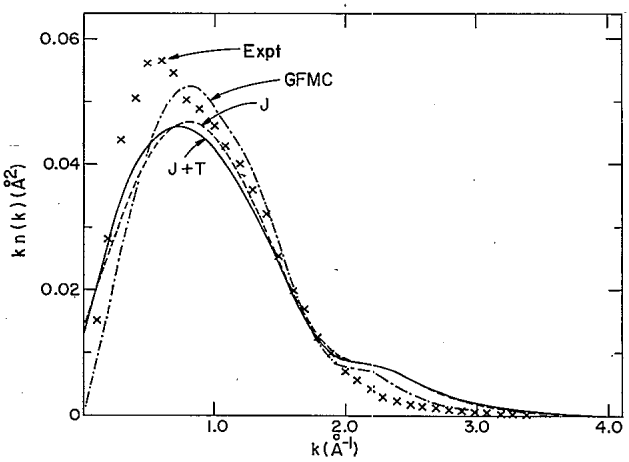

FIG. 8. $n(k)$ is normalized according to Eq. (4.6). The dashed and solid curves are the results of the present calculation with the Jastrow (J) and Jastrow + triplet (J + T) wave function, respectively. The dashed-dotted curve gives GFMC results from Ref. 17. The experimental data (Refs. 3 and 18) are shown with the crosses.

In general we find that the triplet correlation by itself has little effect on the $n(k)$. The $n(k)$ is seen to decrease exponentially for $k > 3$ Å^{-1} in Fig. 7.

The $kn(k)$ obtained from the neutron scattering data[3,18] is compared with theoretical results in Fig. 8. Both the experimental and the GFMC $n(k)$ do not have the correct $k \to 0$ asymptotic behavior. The difference between GFMC and J + T results has to be attributed to (i) the approximations in the use of J + T wave function, and those in the HNC/S calculation; and (ii) the finite box size in the GFMC simulation. The latter effect is particularly manifested at small k. The difference between theory and experiment may be mostly due to the inadequacy of the Aziz potential, or the impulse approximation used in relating the $n(k)$ to neutron scattering cross sections at large momentum transfer. The use of impulse approximation for analysis of scattering from hard core liquids has been recently criticized.[19] There certainly is more

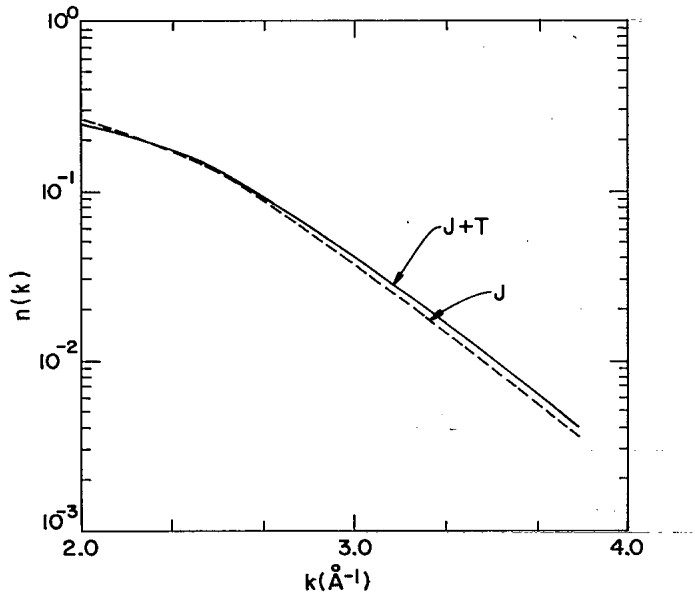

FIG. 7. $n(k > 2$ Å$^{-1})$ of the J and J + T wave functions at $\rho = 0.365\sigma^{-3}$ on log scale. Here $n(k)$ is normalized according to Eq. (2.19).

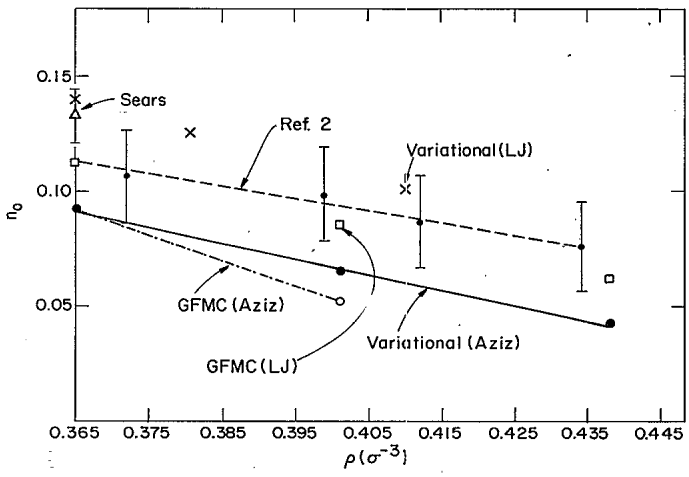

FIG. 9. Comparison of the theoretical and experimental condensate fraction. The solid curve shows the results of this work with Aziz potential. The open circles, joint by a dashed-dotted line, are the results of GFMC calculation with Aziz potential (Ref. 17). GFMC results with Lennard-Jones (LJ) potential are shown with open squares (Ref. 22). The crosses represent the results of Puoskari and Kallio (Ref. 12) variational calculation using LJ potential. The solid circles with the error bars show the data taken from Ref. 2. The dashed line is a guide to the eye. The triangle gives the experimental result at the equilibrium density of Ref. 3.

TABLE III. Results with optimized J and optimized J + T wave functions.

				Condensate fraction			Kinetic energy (K)	
ρ (σ^{-3})	s_{dd}	s_{wd}	s_{ww}	J	J + T	GFMC	T_{MD}(J + T)	T_{JF}(J + T)
0.365	2.44	2.24	2.404	0.098	0.092	0.092	14.86	14.72
0.401	2.78	2.780	2.916	0.071	0.065	0.052	18.17	17.45
0.438	3.12	3.120	3.280	0.048	0.043		22.99	20.53

than qualitative agreement between theory and experiment, marred by significant differences at $k=0.5$ and 2.3 Å^{-1}. The density dependence of the J + T $n(k)$ is given in Table II. The $n(k)$ becomes broader as the density is increased.

The condensate fraction and the kinetic energies are given along with the scaling constants, in Table III. At $\rho=0.438\sigma^{-3}$ the T_{MD} is $\sim 10\%$ larger than the T_{JF} indicating increased importance of the neglected E^t_{xy} diagrams.

The theoretical and experimental condensate fractions are compared in Fig. 9. At equilibrium density and GFMC and J + T values of n_0 are identical, but they are $\sim 20\%$ below the values deduced from neutron scattering experiments. The density dependence of the J + T n_0 is in crude agreement with that of Ref. 2. On the other hand the experiments of Wirth *et al.*[20] have shown no density dependence of n_0, while Mook[21] finds a much stronger decrease in n_0 with ρ.

ACKNOWLEDGMENTS

The authors wish to thank Dr. R. O. Hilleke, Dr. R. M. Panoff, Dr. D. L. Price, Dr. V. F. Sears, Dr. R. O. Simmons, Dr. P. E. Sokol, and Dr. P. A. Whitlock for communicating their results. This work was supported by the U.S. Department of Energy, Division of Materials Sciences, under Contract No. DE-AC02-76ER01198.

*Present address: Department of Physics, Aligarh Muslim University, Aligarh 202001, India.

[1]F. London, Nature (London) **141**, 643 (1938); Phys. Rev. **54**, 947 (1938).
[2]P. E. Sokol, R. O. Simmons, R. O. Hilleke, and D. L. Price (unpublished).
[3]V. F. Sears, Phys. Rev. B **28**, 5109 (1983).
[4]V. F. Sears, E. C. Svensson, P. Martel, and A. D. B. Woods, Phys. Rev. Lett. **49**, 279 (1982); V. F. Sears and E. C. Svensson, Phys. Rev. Lett. **43**, 2009 (1979); A. D. B. Woods and V. F. Sears, Phys. Rev. Lett. **39**, 415 (1977).
[5]M. H. Kalos, M. A. Lee, P. A. Whitlock, and G. V. Chester, Phys. Rev. B **24**, 115 (1981).
[6]R. A. Aziz, V. P. S. Nain, J. S. Carley, W. L. Taylor, and G. T. McConville, J. Chem. Phys. **70**, 4330 (1979).
[7]Q. N. Usmani, S. Fantoni, and V. R. Pandharipande, Phys. Rev. B **26**, 6123 (1982).
[8]S. Fantoni, Nuovo Cimento A **44**, 191 (1978).
[9]M. L. Ristig, P. M. Lam, and J. W. Clark, Phys. Lett. **55A**, 101 (1975); P. M. Lam and M. L. Ristig, Phys. Rev. B **20**, 1960 (1979).
[10]A. Fabrocini and S. Rosati, Nuovo Cimento D **1**, 615 (1982).
[11]Q. N. Usmani, B. Friedman, and V. R. Pandharipande, Phys. Rev. B **25**, 4502 (1982).
[12]M. Puoskari and A. Kallio, Phys. Rev. B **30**, 152 (1984).
[13]Daniel Shiff and Loup Verlet, Phys. Rev. **160**, 208 (1967).
[14]M. H. Kalos, D. Levesque, and L. Verlet, Phys. Rev. A **9**, 2178 (1974).
[15]K. Schmidt, M. H. Kalos, M. A. Lee, and G. V. Chester, Phys. Rev. Lett. **45**, 573 (1980).
[16]L. Reatto and G. V. Chester, Phys. Lett. **22**, 276 (1966).
[17]P. A. Whitlock and R. M. Panoff (unpublished).
[18]V. F. Sears (private communication).
[19]J. J. Weinstein and J. W. Negele, Phys. Rev. Lett. **49**, 1016 (1982).
[20]F. W. Wirth, D. A. Ewen, and R. B. Hallock, Phys. Rev. B **7**, 5530 (1983).
[21]H. A. Mook, Phys. Rev. Lett. **51**, 1454 (1983).
[22]P. A. Whitlock, D. A. Ceperely, G. V. Chester, and M. H. Kalos, Phys. Rev. B **19**, 5598 (1979).